2. THE ENDOHEDRAL FULLERENES $N@C_{60}$, $P@C_{60}$ AND $N@C_{70}$

The first fullerene, C_{60}, was discovered by Kroto et al. in 1985 [44], who received the Nobel Prize for Chemistry in 1996. Although the existence of this highly symmetric molecule was clearly established, there were no macroscopic amounts of it to be investigated until Krätchmer et al. [45] found a way to produce them. Soon afterwards, other fullerene-like molecules were discovered. Later, endohedral fullerenes in which an atom is situated inside the fullerene cage were isolated. The atom inside the molecular trap is usually chemically bonded to the carbon cage and there is a charge transfer between atom and cage. The only known exceptions are the noble gases and the group V atoms in fullerenes, which are not chemically bound and remain in their atomic ground state.
In this chapter the production, enrichment and properties of $N@C_{60}$, $P@C_{60}$ and $N@C_{70}$ will be briefly presented.

2.1 Production by Ion Implantation

$N@C_{60}$ is the first discovered group V endohedral fullerene and was first obtained by Murphy in 1995 [46] using ion implantation. The method is depicted in Fig. 2.1 and will be briefly described. In a vacuum chamber with base pressure around 10^{-6} mbar the fullerenes (a mixture of C_{60}/C_{70}) are sublimed from an effusion cell held at about 500°C, and deposited on a copper plate (target) cooled with liquid nitrogen. At the same time a nitrogen ion beam, generated using a Kaufman source, is focused onto the target, where the ions penetrate the freshly deposited fullerene layer. This process is run continuously for several hours. After implantation, the black powder on the target is dissolved in toluene and remaining carbon soot is filtered out. A mixture of $N@C_{60}/C_{60}$ and $N@C_{70}/C_{70}$ is obtained with a ratio of filled to empty fullerenes of typically 10^{-4}. $P@C_{60}$ is produced using the same procedure [48, 49], the plasma source PH_3 is used instead of N_2. The implantation efficiency is smaller compared with $N@C_{60}$ and the ratio $P@C_{60}/C_{60}$ is about 10^{-5}. Till now $P@C_{70}$ has never been detected, probably because it is not stable enough [49, 47].
In order to simplify the further separation of the fullerenes, the mixed $N@C_{60}/$

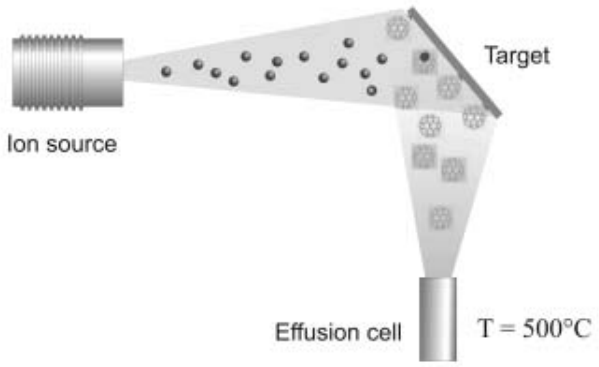

Fig. 2.1: Schematic representation of the ion implantation for the production of group V endohedral fullerenes, after [47].

C_{60} and $N@C_{70}/C_{70}$ ($P@C_{60}/C_{70}$) solution is passed through a plug filter consisting of a silica gel and charcoal mixture with mass ratio 2:1. C_{70} is retained by the filter while C_{60} stays in solution. After the whole amount of C_{60} is washed out, the filtrate is concentrated and ready for the enrichment described below. This procedure leaves the $N@C_{70}/C_{70}$ mixture bound in the plug, and recovery is possible only with a low yield by washing out the plug with other solvents. High Pressure Liquid Chromatography (HPLC) must be used instead of the plug filtration if $N@C_{70}$ material is required. The idea of the latter method is to pass the mixed solution through a column densely packed with SiO_2 grains which have a chemically modified surface. The filling of the column is so dense that a special pump is need to pump the eluent (usually toluene for the fullerene separation) through the column which raises the pressure in the whole system (thus the name of the method). The sample to be separated is injected into the system using a special valve and when the sample runs through the column the different chemical substances have different absorbtion and desorption rates on the column material. In this way the injected mixed solution is separated by the column into two fractions (in the case of two substances) which are monitored after the column by a detector and can be easily collected. The retention time is defined as the time it takes the injected substance to pass through the column minus the time of a substance which is not adsorbed on the column. The retention time depends on the eluent flow rate and on the type of HPLC column. The larger the difference in retention times of the molecules to be separated, the better their separation. Thus the optimal HPLC column, flow rate and injection volume must be found.

2.2 Enrichment

The chemical and physical properties of group V endohedral fullerenes and the related empty fullerenes are considered to be virtually identical. The main difference is of course the presence of the three unpaired p-electrons of the endohedral atom which gives rise to a strong ESR signal. This fact however does not ease the enrichment of the endohedrals. The retention time of C_{60} and $N@C_{60}$ are different but very similar. In the starting material the ratio $N@C_{60}/C_{60}$ is about 10^{-4}, which means that no peak can be observed in the chromatogram as it is covered by the C_{60} peak. The fullerene peak is "cut" into several fractions and the ESR spectrum of each fraction is measured (with identical experimental parameters). The integrated area of the ESR lines gives the number of spins when compared with a spin standard. Afterwards, the best fraction is collected and the process begins again. Using this tedious procedure, 93 % pure $N@C_{60}$ could be produced [50]. The enrichment factor of every step varies between 2 and 10 depending on how the fractions are cut. Usually one does not use the largest possible enrichment factor is used since in this fraction there is too little $N@C_{60}$. Therefore an optimal cutting strategy must be found. In order not to lose too much material during the further enrichment steps, peak recycling is used. The basic idea is not to collect fractions but to re-inject the "peak" and to let it pass again through the column. After about 10 cycles the pure $N@C_{60}$ is let out of the system and another sample is injected [50].
The purification of $P@C_{60}$ is done with the same HPLC setup and using the same experimental parameters - flow rate and injection volume. However the enrichment factor is higher and varies from 30 to 100, again depending on the cutting strategy of the fractions. In earlier studies the material was enriched up to a few percent [47]. One of the purposes in this work was the further enrichment of $P@C_{60}$, possibly up to 100 %, which however seems to be extremely difficult. The reconstruction of the HPLC peak of $P@C_{60}$ from this study is shown in Fig. 2.2. The first two HPLC steps enriched the $P@C_{60}/C_{60}$ ratio from 10^{-5} about to 5% with enrichment factor 70 in each step. It was expected that the next HPLC run would provide pure $P@C_{60}$ but this was not the case. The chromatogram of the best achieved $P@C_{60}$ sample is shown in Fig. 2.3 where the corresponding concentration is 20 %. Unfortunately pure $P@C_{60}$ could not be obtained, even when its peak was selectively cut and the corresponding fraction collected. The latter was again injected but the resulting chromatogram was still similar to the one shown in Fig. 2.3. An additional peak is observed before the C_{60} peak with unknown origin, possibly some product of the decomposition of $P@C_{60}$. Similar deviations of nearly pure $N@C_{60}$ from the usual behavior of $N@C_{60}/C_{60}$ mixture with lower concentrations were observed in other

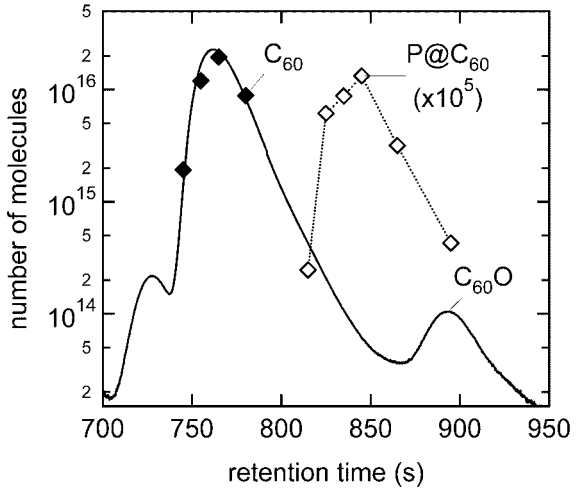

Fig. 2.2: Reconstruction of the $P@C_{60}$ peak (dashed line) in the preparative chromatogram (solid line) using optical absorbtion (full squares) and ESR data of each gathered fraction (empty squares).

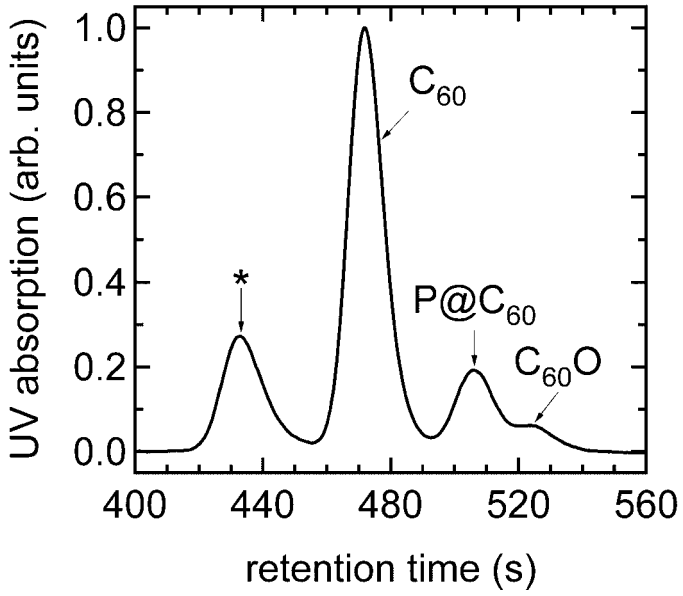

Fig. 2.3: Chromatogram of 20 % enriched $P@C_{60}$. The peak denoted with * has unknown origin, possibly from a chemical reaction between the highly enriched material and the material in the HPLC column.

groups [50]. It is possible that N@C_{60}, and even more likely that P@C_{60}, react with the Buckyprep column material. At lower concentrations this reaction would be hindered by the presence of empty C_{60} on the column.

2.3 Properties

The spin Hamiltonian for the endohedral atom can be deduced from equation (1.6) omitting H_{ZFS} and is written like:

$$H_{spin} = H_{ZI} + H_{HI} = \hbar\omega_0 S_z + \hbar\, 2\pi a(S_x I_x + S_y I_y + S_z I_z) \tag{2.1}$$

The terms aS_xI_x and aS_yI_y can be omitted considering the high symmetry of the molecule and if the hyperfine interaction is taken to first order. Second order effects can be observed in spectra from solution [51] and can lead to a Electron Spin Echo Envelope Modulation (ESEEM) [52]. The level scheme and typical spectra of P@C_{60} are shown in Fig. 2.4 and those of N@C_{60} in Fig. 2.5.

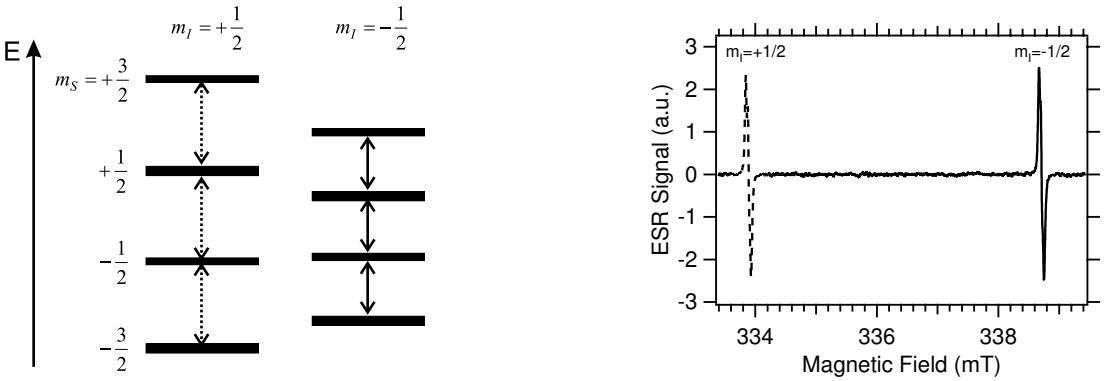

Fig. 2.4: Energy levels for P@C_{60} in a constant magnetic field (left). Only two spectral lines (right) are observed and the corresponding transitions are marked with solid and dashed arrows. The spectrum is of a solid state sample measured at room temperature with a field modulation amplitude of 15 μT and MW power 0.316 mW (25 dB attenuation).

The energy values can be calculated using the expression:

$$E_{m_S,m_I} = m_S\hbar\omega_0 + m_I m_S \hbar 2\pi a$$

where $m_S = -\frac{3}{2}, -\frac{1}{2}, +\frac{1}{2}, +\frac{3}{2}$, $m_I = +\frac{1}{2}, -\frac{1}{2}$ for P@C_{60} and $m_I = -1, 0, +1$ for N@C_{60}. The spectral lines are extremely narrow (FWHH about 200 kHz) if compared to usual ESR lines (FWHH > 1 MHz). This fact allows the observation of second-order hyperfine splitting in solution ESR spectra of N@C_{60} and P@C_{60}. The hyperfine constant a is isotropic and positive (except for 15^N where $a < 0$) and

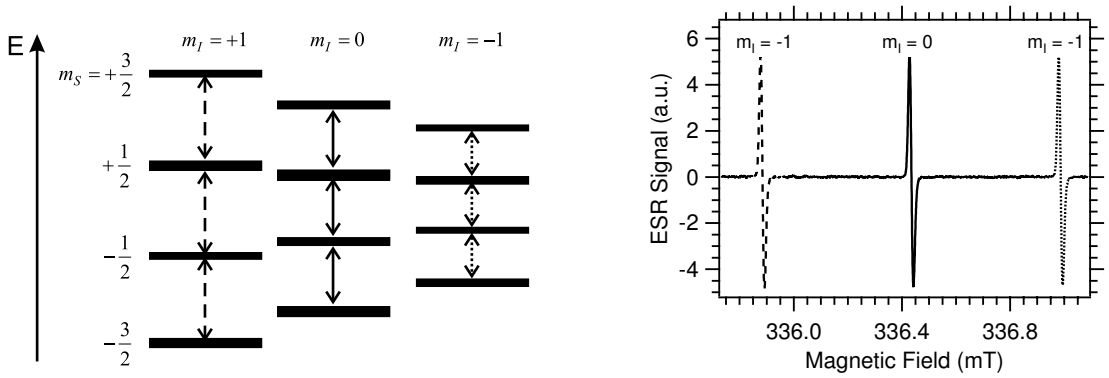

Fig. 2.5: Energy levels for N@C_{60} in a constant magnetic field (left). Three spectral lines (right) are observed and the corresponding transitions are marked with solid and dashed arrows. Solid state sample at room temperature was measured using modulation amplitude 10 μT and MW power 0.0316 mW (35 dB attenuation).

values for different atoms encapsulated in fullerenes and free atoms are compared in table 2.1. An increase of the hyperfine constants is observed when N and P atoms

endohedral	$\|a\|$ (MHz)	$\|a\|$ free atom (MHz)
^{14}N@C_{60}	15.73 [46]	10.45 [53]
^{14}N@C_{70}	15.106 [51]	10.45 [53]
^{15}N@C_{60}	22.021 [46]	14.64 [54]
P@C_{60}	137.76 [49]	55.02 [55]

Tab. 2.1: Comparison of the hyperfine constants for N and P as free atoms and in C_{60} and C_{70}.

are trapped in the fullerenes, suggesting that the atomic orbitals of the endohedral atom are "squeezed". Different quantum chemical calculations [56, 57] show that there is no significant interaction (wave function overlap) between the endohedral atom and the carbon cage. The natural abundance of ^{13}C (nuclear spin 1/2) is about 1.07 % thus there is one C_{60} atom on every second cage. Therefore coupling between the electron spin of the endohedral atom and the carbon 13 nuclear spin is expected and experimentally detected [58]. The super hyperfine constant is $a_{^{13}C} = 32$ kHz.
A small g-factor shift about 19 ppm (65 mG) is observed for N@C_{70} compared to N@C_{60}, which is attributed to the different ring currents in C_{70} and C_{60} [51]. It is possible to detect this effect only because of the extremely narrow ESR lines of N@C_{60} and N@C_{70}. The chemical shift (about 22 ppm) in NMR spectra of He@C_{70} and He@C_{60} [59] is very close to the one of the nitrogen endohedrals.

2.3.1 Quadrupole Echo

Polycrystalline P@C_{60} shows a zero field splitting (ZFS) at $T = 10$ K which broadens the bottom part of the ESR lines as it can be seen in the echo detected spectrum

shown in Fig. 2.6. Such a spectrum is taken when the Hahn echo sequence is applied

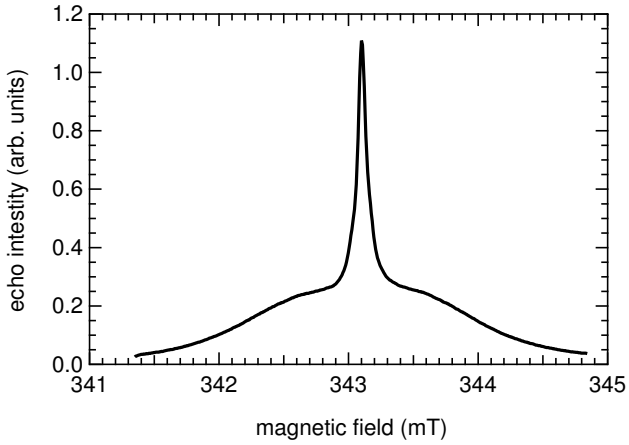

Fig. 2.6: Echo detected spectrum of polycrystalline P@C_{60} at $T = 10$ K, adapted from [47]

(see Fig. 1.2) and the magnetic field is swept. The spectrum can be simulated with the MatLab package Easy Spin [60] with a value for the ZFS $D = 19.5$ MHz with a very broad Gaussian distribution of the ZFS $\delta D = 24$ MHz. Nutation experiments at $T = 10$ K reveal a similar value $D \approx 18.2$ MHz again with a large δD [47] while at room temperature D decreases to 6.72 MHz. The observed spectral lines come only from a transition with $m_S = +1/2 \leftrightarrow m_S = -1/2$, i.e. the transitions with $m_S = 3/2 \leftrightarrow m_S = 1/2$ and $m_S = -1/2 \leftrightarrow m_S = -3/2$ could not be detected. In the present work the non-vanishing value of the ZFS was treated (at $T = 10$ K) by analyzing the form of the Hahn echo shown in Fig. 2.7. This signal corresponds to

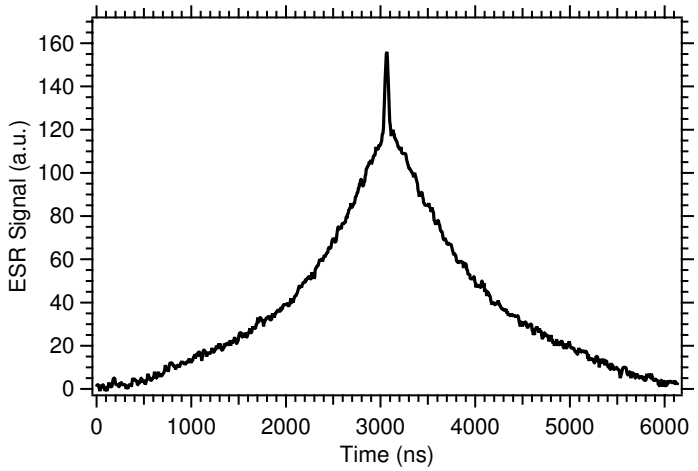

Fig. 2.7: Echo of polycrystalline P@C_{60} at $T = 10$ K.

the well known quadrupole echo in NMR for nuclear spins with $I > 1/2$ with non-vanishing quadrupole moments Q [33]. The quadrupole interaction Hamiltonian is

written like:

$$H_Q = \frac{1}{2}\hbar\omega_Q\Big[I_z^2 - \frac{1}{3}I(I+1)\Big] \tag{2.2}$$

with

$$\omega_Q = \frac{3eQV_{zz}}{2I\hbar(2I-1)} \tag{2.3}$$

where e is the elementary charge, Q is the quadrupole moment of the nucleus and V_{zz} is the electric field gradient along the z axis (see for example [61]). In the case of ESR the fine structure interaction Hamiltonian is used which equals (2.2) if ω_Q is replaced by D. The echo signal expected for such a Hamiltonian can be divided into two parts - magnetic and quadrupole [33]:

$$S \approx C_Q + C_M = \frac{9}{5}\cos^2(\beta/2)\sin^4(\beta/2)\cos(\omega_Q t) + \frac{1}{10}\cos^2(\beta/2)[3\cos(\beta)-1]^2 \tag{2.4}$$

here β is the turning angle of the second MW pulse. In the Fourier transform of the echo signal two peaks are expected. First a large peak at frequency $\nu_0 = 0$ can be assigned to the magnetic echo and a second one with smaller intensity at $\nu_Q = \omega_Q/2\pi$ $(2D)$ according to equation (2.4). In the case of a polycrystalline sample there is random orientation of the different crystallites with respect to the applied magnetic field and then $\nu_Q = D$ [62]. The Fourier transform of the quadrupole echo of polycrystalline P@C_{60} measured at $T = 10$ K is shown in Fig. 2.8. The obtained

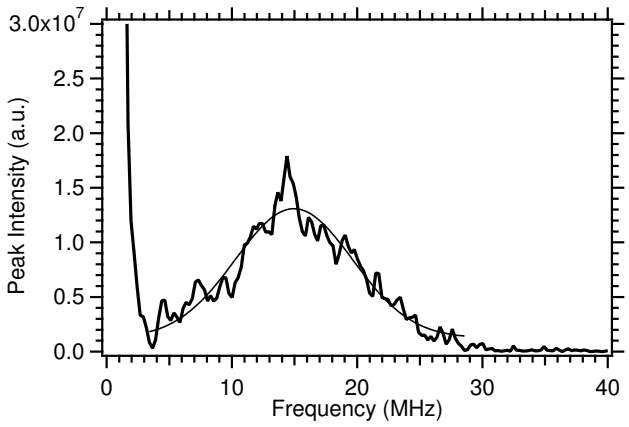

Fig. 2.8: Fourier transform of the quadrupole echo of polycrystalline P@C_{60} at $T = 10$ K. The solid line is a Gaussian fit with $\nu_Q = 15.0(1)$ MHz and width $\delta\nu_Q = 11.0(6)$ MHz.

here values for $D = 15.0(1)$ MHz and $\delta D = 11.0(6)$ MHz are lower then the values extracted from nutation experiments. The same trend that $D \approx \delta D$ is observed. The presence of zero field splitting D is a hint for lowering of the symmetry of the fullerenes cage, the latter being chemically unmodified.

2.4 Chemical Modification

$N@C_{60}$ and $N@C_{70}$ are stable below 500 K, while $P@C_{60}$ decomposes at even lower temperatures (but still above room temperature) [63]. The exact process of degradation is not yet known, only constant loss of the spin signal is observed by heating the endohedrals above 500 K and also when they are stored under day light. The poor thermal stability limits the possible chemical reactions of the endohedrals, but there are still some that work at room temperature or slightly above. The first reported chemical modification of $N@C_{60}$ is the Bingel-type reaction [64] with diethylmalonyl bromide to the monoadduct $N@C_{60}C(COOC_2H_5)_2$ [65]. The nitrogen atom stays inside the cage and its lowered symmetry gives rise to a ZFS of $D_{eff} = 6.1$ MHz. Two extra lines for each hyperfine line [65] can thus be observed in polycrystalline samples. No change or anisotropy of the hyperfine constant a and of the g-factor was observed. Up to six functional groups have been attached to the carbon cage [66]. The ESR spectra of the hexaadduct shows again only the three lines of $N@C_{60}$ because the fullerenes cage has recovered its symmetry. It is interesting to note the higher thermal stability of the hexaadduct compared to the unmodified $N@C_{60}$ [66]. A possible mechanism of the decomposition of $N@C_{60}$ is that first the endohedral atom binds to the carbon cage and then it moves outside the fullerene. In the hexaadduct there are less double bonds with which the nitrogen atom can bind and the escape reaction is blocked.

The first chemical modification of $P@C_{60}$ was done in our group and it is again the Bingel type reaction with dimethyl malonate chloride and diethyl malonate [67]. The room temperature ESR spectra of both adducts are shown in Fig. 2.9. Unlike the chemically modified $N@C_{60}$, no ZFS is observed even at low temperatures, which is quite surprising because the p-wave function of the phosphorus in C_{60} is more "squeezed" (the hyperfine constant of $P@C_{60}$ is 2.5 times larger compared to the "free" phosphorus atom, see table 2.1 than that of $N@C_{60}$ and it should be more sensitive to variations of the symmetry of fullerene cage. Moreover as polycrystalline, unmodified $P@C_{60}$ shows ZFS at low temperatures (see previous section), it was expected that its chemical modification would give rise to an even larger ZFS. The splitting of each ESR line in the spectra of the adducts can not be explained by ZFS because position and shape of the lines do not correspond to those expected for a ZFS powder pattern. The second order hyperfine interaction ($a^2/2B_0$) can also not cause the observed line shapes since its value of 36 μT is too small to be seen in these spectra width a line width of 100 μT (240 μT). In order to interpret the experimental data, a simulation with the Easy Spin package [60] was done but it reproduces the data only qualitatively.

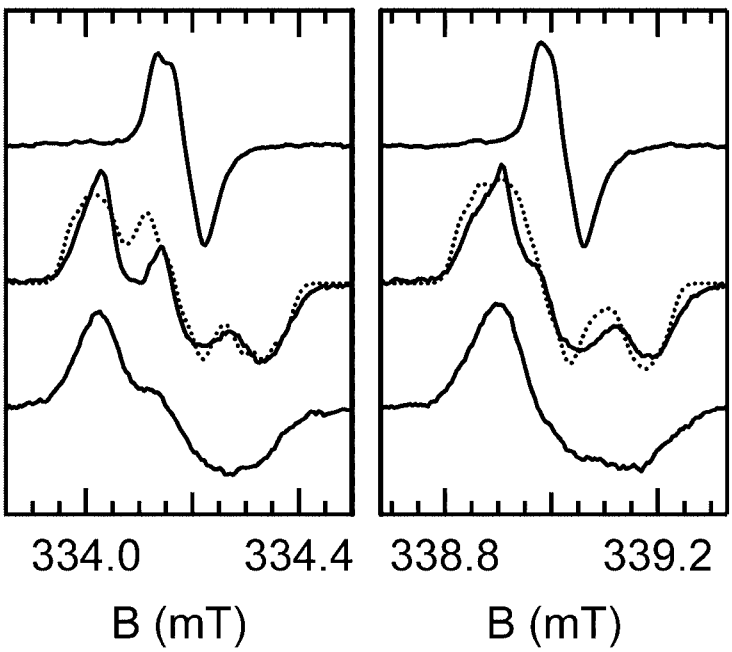

Fig. 2.9: The low field (left) and high field ESR line of P@C_{60} (top), methyl-malonyl adduct (middle) and ethyl-malonyl adduct (bottom) [67]. The dotted line is a simulation.

The broader lines of the ethyl substituted malonate suggest stronger coupling to the protons of the malonate, but both have similar line shapes and the broadening is only 50 μT. Thus anisotropic proton coupling alone is unlikely to explain the line shapes. The ESR properties of the chemically modified N@C_{60} and P@C_{60} are summarized in table 2.2

The best fit was obtained with an anisotropic g-factor and an anisotropic hy-

endohedral	a (MHz)	g-factor	l.w. (MHz)	source
^{14}N@C_{60}	15.73	2.003	0.448	[46]
^{14}N@C_{60}C(COOEt)$_2$	15.73	2.003	1.316	[66]
^{14}N@$C_{60}C_6$(COOEt)$_{12}$	15.73	2.003	2.38	[66]
^{14}N@C_{60}-C_{60}	15.55	2.003	1.68	[68, 47]
P@C_{60}C(COOEt)$_2$	anisotropic [a]	anisotropic[a]	6.7	this work
P@C_{60}C(COOMe)$_2$	anisotropic[a]	anisotropic[a]	2.82	this work

[a] The g factor and the hyperfine constant values used to simulate the ESR spectra are anisotropic with $g = (g_{xx}, g_{yy}, g_{zz}) = (2.0024, 2.0022, 2.00225)$ and $A = (A_{xx}, A_{yy}, A_{zz} = (135, 145, 127)$

Tab. 2.2: ESR properties of chemically modified N@C_{60} and P@C_{60} (powder samples measured at room temperature in X-band).

perfine constant A with diagonal elements $g = (2.0024, 2.0022, 2.00225)$ and $A = (135, 145, 127)$ MHz, shown in Fig. 2.9 as a dotted line. Such an anisotropy has

never been measured in chemically modified N@C_{60} (see table 2.2) and the apparent absence of ZFS from the simulation is puzzling. It is possible that there is a fine structure D but its distribution has to be much broader than in polycrystalline P@C_{60}. This would cause such a strong decrease of the intensity of the expected satellite line due to the transitions $|+3/2\rangle \leftrightarrow |+1/2\rangle$ and $|-1/2\rangle \leftrightarrow |-3/2\rangle$ (see the next chapter), that they could disappear under the noise level. A definitive identification of the transitions would be possible with transient nutation experiments. The sample size however was too small for pulsed experiments in X-band.
Pulse ESR measurements of modified P@C_{60} were done in W-Band at room temperature and below. Unexpectedly the CW ESR spectra depicted in Fig. 2.10 show only two hyperfine lines which are not split as in X-Band. The line width is reduced

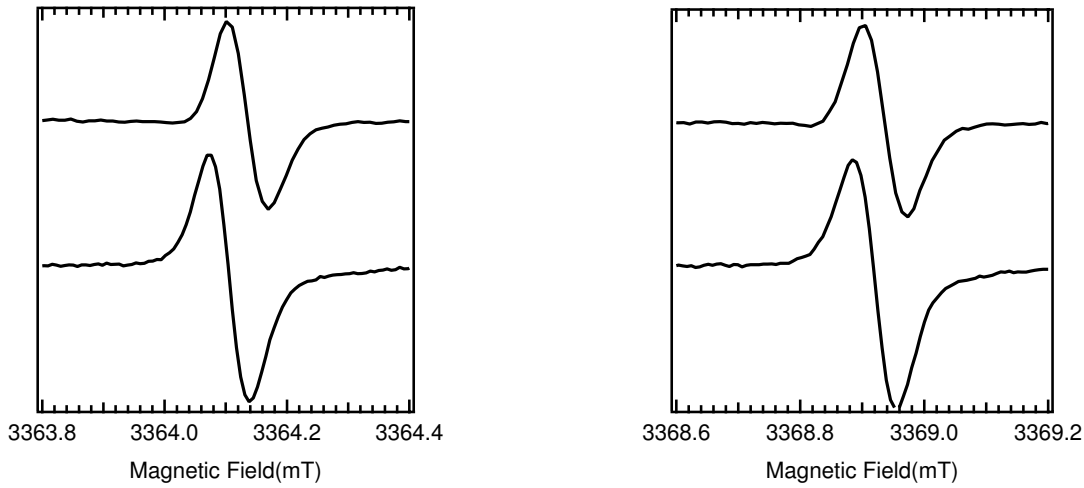

Fig. 2.10: The low field (left) and high field (right) ESR line of methyl-malonyl (top) and ethyl-malonyl (bottom) P@C_{60} adducts.

to 2.53 MHz and 2.06 MHz for the ethyl- and methylmalonate adduct respectively. If there is anisotropy of the g factor as was assumed for the simulation above, a much larger separation of the lines in W-Band is expected because of the higher magnetic field B_0. Anisotropy of the hyperfine constant a must be also measurable at W-Band since a does not depend on the applied magnetic field. Both expectations were not confirmed in these experiments. The idea that the samples were decomposed before the experiments was rejected as they were again measured in X-band and showed the same spectra. Until now no reasonable explanation was found to explain these data.
The spin-lattice relaxation time T_1 and spin-spin relaxation time T_m (see chapter 1.5.6 and 4 for definition) for the ethylmalonate derivative were found to be correspondingly 8.4 and 3.2 μs at room temperature. The values for the methylmalonate adduct are 9.7 and 4.6 μs while at $T = 50$ (100) K, T_m was measured to

be 14.8 (15.4) μs. These results show that the chemical modification of P@C_{60} does not influence its relaxation properties very much. The latter will be discussed in more detail in chapter 4.

2.5 Conclusions

The production of N@C_{60}, N@C_{70} and P@C_{60} by ion implantation and the subsequent HPLC enrichment was descried. P@C_{60} was purified up to 30 % for the first time but all attempts to obtain pure material were so far unsuccessful, possibly due to its decomposition during the enrichment. In the chromatogram the P@C_{60} peak can be clearly seen together with a peak of unknown origin which is assigned to a product of the degraded P@C_{60}.

The encapsulated atom in the group V endohedral fullerenes is in its atomic ground state with electron spin $S = 3/2$. The corresponding ESR spectra show sharp lines even at room temperature with no resolved fine structure. The value of the hyperfine constant is always larger than in the "free" atoms indicating the "squeezing" the atomic orbitals of the endohedral atom. The echo signal of polycrystalline P@C_{60} at low temperatures has the form of a quadrupole echo due to non-vanishing ZFS. The analysis of the echo signal reveals values for the ZFS D and its Gaussian distribution δD correspondingly 15.0(1) and 11.0.

Chemical modification of N@C_{60} lowers the symmetry of the carbon cage thus lifting the degeneracy in the electrons spin energy levels. The resulting ESR spectra show well resolved fine structure with $D = 6$ MHz. It was found that P@C_{60}, despite of its lower than N@C_{60} thermal stability, can also build adducts. The X-band ESR spectra show no ZFS and anisotropy in g and A was used to simulate the observed spectra. This result is unexpected since P@C_{60} is more sensitive than N@C_{60} to cage deformations. Surprisingly, CW W-band spectra reveal only two hyper fine lines with no anisotropy in g, while the latter was expected to increased due to the larger magnetic field. Spin-lattice and spin-spin relaxation times T_1 and T_2 could be measured only in W-band due to small sample size. T_1 and T_2 values are found to be similar as in the bulk polycrystalline P@C_{60}.